AAAS
Ultrafast Science
Volume 2021, Article ID 9837107, 12 pages
https://doi.org/10.34133/2021/9837107

Ultrafast Science
A SCIENCE PARTNER JOURNAL

Research Article

Ultrafast Hole Deformation Revealed by Molecular Attosecond Interferometry

Yindong Huang,[1,2] **Jing Zhao**,[1] **Zheng Shu**,[3] **Yalei Zhu**,[1] **Jinlei Liu**,[1] **Wenpu Dong**,[4] **Xiaowei Wang**,[1] **Zhihui Lü**,[1] **Dongwen Zhang**,[1] **Jianmin Yuan**,[1,5] **Jing Chen**,[3,6] **and Zengxiu Zhao**[1]

[1]*Department of Physics, National University of Defense Technology, Changsha, Hunan, China*
[2]*Innovation Laboratory of Terahertz Biophysics, National Innovation Institute of Defense Technology, Beijing, China*
[3]*Institute of Applied Physics and Computational Mathematics, Beijing, China*
[4]*Hypervelocity Aerodynamics Institute, China Aerodynamics Research and Development Center, Mianyang, Sichuan, China*
[5]*Graduate School of China Academic of Engineering Physics, Beijing, China*
[6]*Shenzhen Key Laboratory of Ultra Intense Laser and Advanced Material Technology, Center for Advanced Material Diagnostic Technology, and College of Engineering Physics, Shenzhen Technology University, Shenzhen, China*

Correspondence should be addressed to Jianmin Yuan; jmyuan@nudt.edu.cn, Jing Chen; chen_jing@iapcm.ac.cn, and Zengxiu Zhao; zhao.zengxiu@gmail.com

Received 25 March 2021; Accepted 7 May 2021; Published 7 July 2021

Understanding the evolution of molecular electronic structures is the key to explore and control photochemical reactions and photobiological processes. Subjected to strong laser fields, electronic holes are formed upon ionization and evolve in the attosecond timescale. It is crucial to probe the electronic dynamics in real time with attosecond-temporal and atomic-spatial precision. Here, we present molecular attosecond interferometry that enables the *in situ* manipulation of holes in carbon dioxide molecules via the interferometry of the phase-locked electrons (propagating in opposite directions) of a laser-triggered rotational wave packet. The joint measurement on high-harmonic and terahertz spectroscopy (HATS) provides a unique tool for understanding electron dynamics from picoseconds to attoseconds. The optimum phases of two-color pulses for controlling the electron wave packet are precisely determined owing to the robust reference provided with the terahertz pulse generation. It is noteworthy that the contribution of HOMO-1 and HOMO-2 increases reflecting the deformation of the hole as the harmonic order increases. Our method can be applied to study hole dynamics of complex molecules and electron correlations during the strong-field process. The threefold control through molecular alignment, laser polarization, and the two-color pulse phase delay allows the precise manipulation of the transient hole paving the way for new advances in attochemistry.

1. Introduction

Since the late 1980s, time-resolved femtosecond techniques have led to tremendous developments in observing and manipulating chemical reactions at a timescale shorter than the period of vibration and rotation, i.e., to form or break chemical bonds in real time [1–4]. However, if viewed from a faster and a more microscopic scale, a chemical reaction originates from the overlap and departure of electron wave packets (EWPs) [5–8]. Nowadays, advances in ultrafast science have enabled the detection of these dynamics by pulses or time-resolved gating with attosecond precision [9–11]. Coupling among electrons or between nuclei and electrons helps to realize a subfemtosecond-timescale manipulation of electron and hole dynamics [12, 13], which is pivotal for controlling the chemical reactions that follow. For instance, a redox reaction is an ultrafast process of gaining and losing electrons [14]. Manipulation of these electrons can migrate a localized charge, thereby forming new chemical bonds between molecules [15].

The natural spatial-temporal scale of electrons is at the atomic and molecular levels, which can be used to self-probe the dynamics of a hole and EWPs in a controlled fashion [16, 17]. In the strong laser fields, EWPs disperse in space

after ionization and can recombine with the parent ion to emit high-energy photons: all of these occur consecutively within a laser cycle [18]. Since this process is induced by a highly nonlinear tunneling ionization, instant removal or excitation of an electron can provide a strong mixture of many one-hole configurations: an electron missing in the highest occupied molecular orbital (HOMO) or an electron missing in the inner orbitals [19]. The wave packet of a hole, therefore, exhibits a time-dependent periodic flow with a period $T = \hbar/\Delta E$, where ΔE is the energy spacing between the two states [20, 21]. Controlling the periodic flow of EWP offers a unique possibility of steering chemical reactions within the timescale of electrons.

In this article, we demonstrate a new methodology to pump and probe a hole from different molecular alignments, enabling the visualization of the ultrafast hole deformation using molecular attosecond interferometry. Threefold control is achieved here: First, an alignment pulse is used to excite the rotational wave packet, resulting in the field-free alignment of molecules at a later time delay. The rotational wave packet can be traced by monitoring the intensities of harmonics generated by a delayed probing pulse to pinpoint the moment of alignment [23, 24], as shown in Figure 1(a) for the ensemble of CO_2 molecules. Second, the attosecond-scale EWPs are manipulated by using a two-color laser pulse to form attosecond interferometry. Analogous to Young's spatial two-slit interferometry, we construct a temporal interferometry within one laser cycle by perturbing the dynamics of the EWPs propagating in opposite directions (Figure 1(b)) [25, 26]. Third, by varying the polarization between the two-color laser pulse and the alignment pulse, the hole along different angles in the molecular frame can be created as needed. Since the ionization of molecules is channel-dependent, hole deformation strongly depends on the molecular orbitals involved [21]. For instance, due to the nodes of HOMO, ionization from HOMO will be greatly suppressed; thus, the inner orbitals will become vital at specific angles [27]. The third control, therefore, completes molecular attosecond interferometry by manipulating the amplitude and relative phase between different channels and, in turn, providing hole control, as shown in Figure 1(c). The shape of the hole can be encoded by the recombined EWP [28] and reflect itself on the harmonic and terahertz (THz) emission spectra.

The threefold control involves different timescales from picoseconds to attoseconds, allowing us to observe the interplay between different ionization channels and the resultant complex electron-hole dynamics by comparing with the theoretical model and *ab initio* calculations. In addition, the yield and modulation of the accompanying THz emission can help to characterize the alignment-dependent ionization probability [29] and relative phase of the two-color laser fields [30], facilitating the identification of different channels during hole formation. The technology established in this work pushes the precise and multidimensional control of electron/hole dynamics into a new level and can be generalized to address the electron correlations in more complex systems. Moreover, varying the alignments and the two-color phases can modulate the hole wave packet and EWP of molecules, therefore resolving and controlling the nuclear dynamics and the chemical bonds [31].

2. Materials and Methods

2.1. Experimental Design. Figure 2(a) shows the scheme of molecular attosecond interferometry and its general probing mechanism. The experimental setup consists of a Ti:sapphire system (100 fs, 800 nm, 4.4 mJ, and 1 kHz) and vacuum charmers for the generation and collection of high-harmonic and terahertz spectroscopy (HATS) from laser-aligned CO_2. The second-harmonic (400 nm) pulse is introduced by a 30 μm type-I β barium borate (β-BBO) crystal, and it collinearly propagates with the fundamental pulse to keep the two-color relative phase stable. The phase difference between the two-color pulses is compensated by an α-BBO crystal and can be precisely adjusted by a pair of fused silica wedges. The intensity of the second-harmonic pulse is roughly varied by tilting the pitching angle of the β-BBO. A wire grid polarizer is placed on the generation arm to ensure linear polarization before focusing. The typical intensities of the aligning pulse, the fundamental pulse, and the second-harmonic pulse in the experiment are estimated as 7×10^{13} W/cm^2, 2×10^{14} W/cm^2, and 2×10^{12} W/cm^2, respectively. The alignment angle α', which is the angle between the alignment pulse polarization and the generation pulse, can be continuously varied by a rotatable half-wave plate. A homemade continuous nozzle (200 microns in diameter) is placed 0.2 mm above and 2 mm after the focus of the generating beam with 1 bar backing pressure. The rotational temperature of the molecule ensemble is estimated to be 90 K and the maximum of $\langle \cos^2\theta \rangle$ at the alignment moment is about 0.67. Each high-harmonic spectroscopy (HHS) accumulates 3000 pulses by an X-ray CCD. The THz waveform is detected by one 1 mm thick (110)-cut ZnTe crystal via electrooptic sampling (EOS).

3. Results

3.1. Ionization Determined by THz Detection. When a weak second-harmonic pulse is added, an additional phase between the consecutive half-cycles of the Michelson interferometry breaks the time-reversal symmetry of the EWPs and leads to the generation of even harmonics (Figure 2(b)) [25] and the THz wave (Figure 2(c)) [30]. Because they are inherently phase-locked from strong field interactions, the joint measurement of HATS offers an unusual opportunity to observe electron or hole dynamics in multiple dimensions. For instance, the molecular alignment can be monitored by tracing the harmonic yield, which varies with the time delay t_D between the aligning pulse and the generation pulse. The transient rotational wave packets of the alignment and antialignment ensembles are sketched in the inset of Figure 1(a). The following experiments were carried out when t_D is 21.3 ps, i.e., the alignment moment around the half-revival of CO_2 rotational wave packet [32].

As demonstrated in our previous work, the measured THz yield can serve as a reference to angular differential

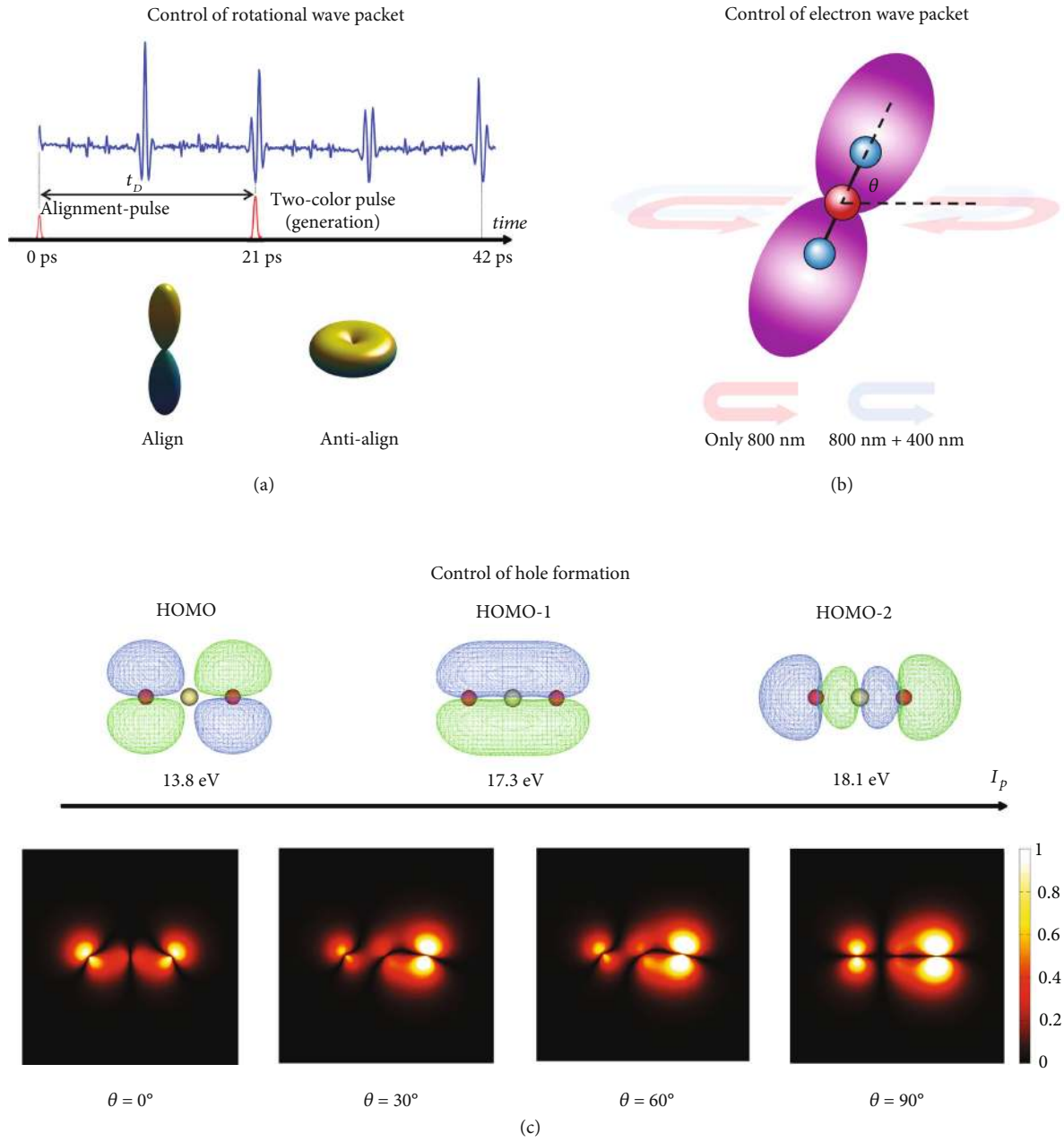

FIGURE 1: Threefold control of molecular attosecond interferometry. (a) Control of molecular rotation. Experimental yield of the harmonic 25th from CO_2 as a function of the alignment and generation pulse delay t_D. The two figures in the bottom sketch the calculated rotational wave packet at the alignment ($t_D \simeq 21.3$ ps) and antialignment ($t_D \simeq 21.7$ ps) moments. (b) Control of attosecond electron wave packet. The arms on the left and right sides of the electron wave packet are constructed by the adjacent half-cycles of the laser. Two symmetric trajectories are generated by using only the fundamental laser pulse (red trajectories), while adding the second-harmonic pulse can break the symmetry (blue trajectories) and introduce the even harmonics and THz emissions. θ is the direction of molecular axis with respect to the generation pulse polarization. (c) Control of hole formation. The calculated HOMO, HOMO-1, and HOMO-2 orbitals are shown with their binding energies, respectively [22]. Ionization of molecules is strongly dependent on the molecular orbitals involved. The angle-resolved hole wave packet in the molecular frame can be reconstructed by EWPs propagating in opposite directions to exhibit the deformation of a hole and therefore, under different azimuth angle θ, form molecular attosecond interferometry (data from H28).

ionization probability [29]. In Figure 2(d), alignment-dependent THz yields (averaged over eight independent measurements) are depicted under two relative phases ϕ between the two-color laser fields with fixed intensity ratios. The alignment-dependent THz yields maintain a similar shape under different relative phases, and both peak at 42 $\pm$ 2 degrees. This agrees with the previous ion measurements [33, 34] but differs from the theoretical predictions [35–37].

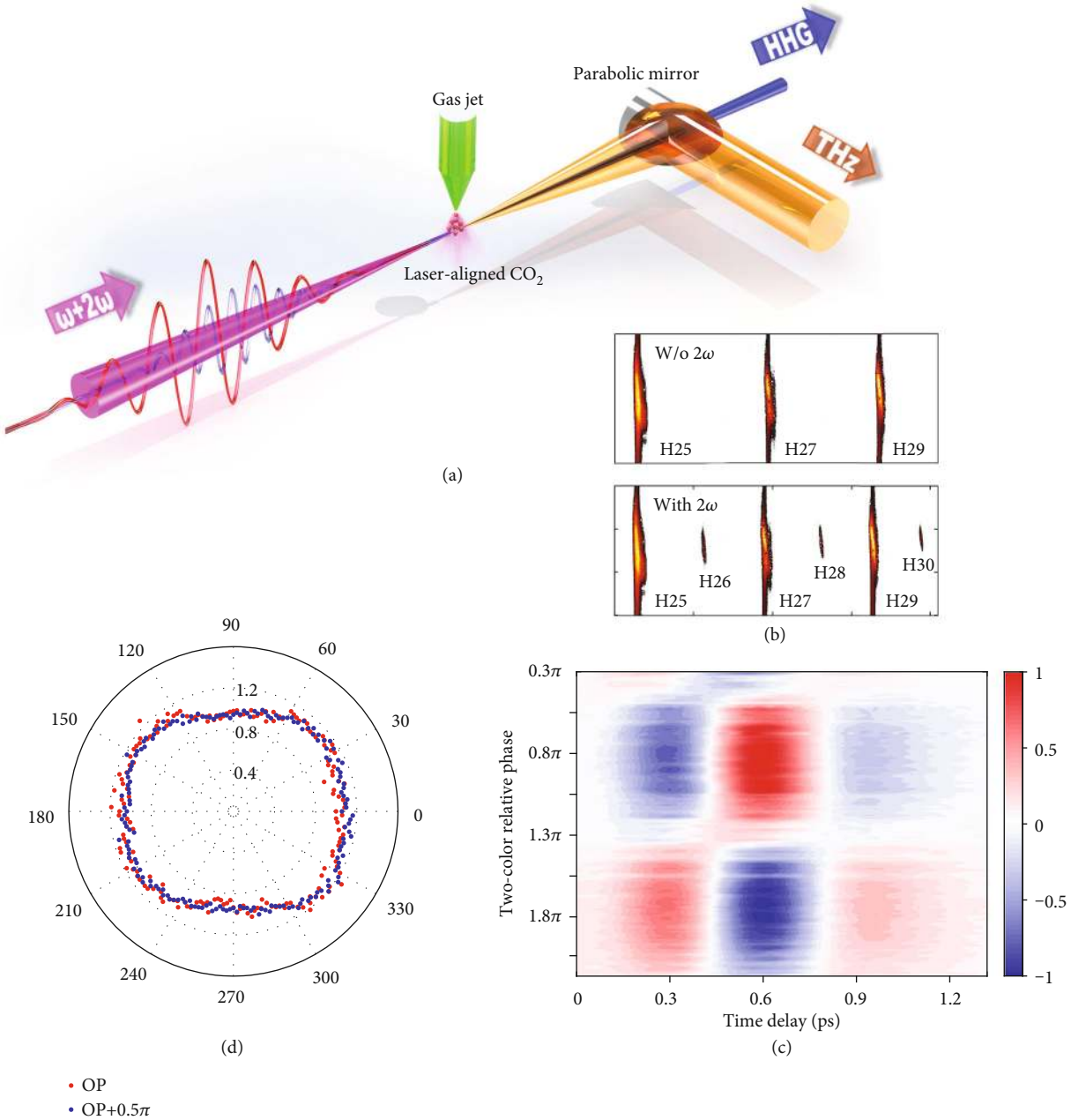

FIGURE 2: Joint measurements of high-harmonic and terahertz spectroscopy (HATS). (a) Schematic illustration of the experimental setup of HATS. ϕ is the phase delay between two-color fields. (b) CCD camera images (pseudocolor) of high-harmonic spectroscopy with or without the second-harmonic pulse. (c) Normalized terahertz waveforms as a function of ϕ and time delay for electrooptic sampling (EOS). (d) Alignment-dependent terahertz yields at the optimal two-color phase delay (OP, red dots) and OP+0.5π (blue dots). The scanning angle step of the alignment angle is 2 degrees.

Recent theoretical advances show that dynamic exchange of electrons is indispensable for addressing the differential ionization property of polyatomic molecules [38]. By continuously varying the relative phase between two-color fields, we find that the modulation of THz yields under different alignments is hard to change, as illustrated in the bottom row of Figure 3(a). This result suggests that the alignment angle α' and the two-color relative phase ϕ are decoupled in THz generation from CO_2. The intensity of the THz wave generated from aligned molecules, therefore, can be expressed as a product of the alignment-dependent THz yields and a modulation function of the two-color phase delay,

$$I_{\mathrm{THz}}\left(\alpha';\phi\right) \simeq \left[E_{\mathrm{THz}}\left(\alpha'\right)\cos\left(\phi-\phi_{\mathrm{op,T}}\right)\right]^2 \propto N^2\left(\alpha'\right)\cos^2\left(\phi-\phi_{\mathrm{op,T}}\right), \quad (1)$$

where $\phi_{\mathrm{op},T}$ is the optimal two-color phase (OP) for the maximal THz yields. Meanwhile, the alignment-dependent THz

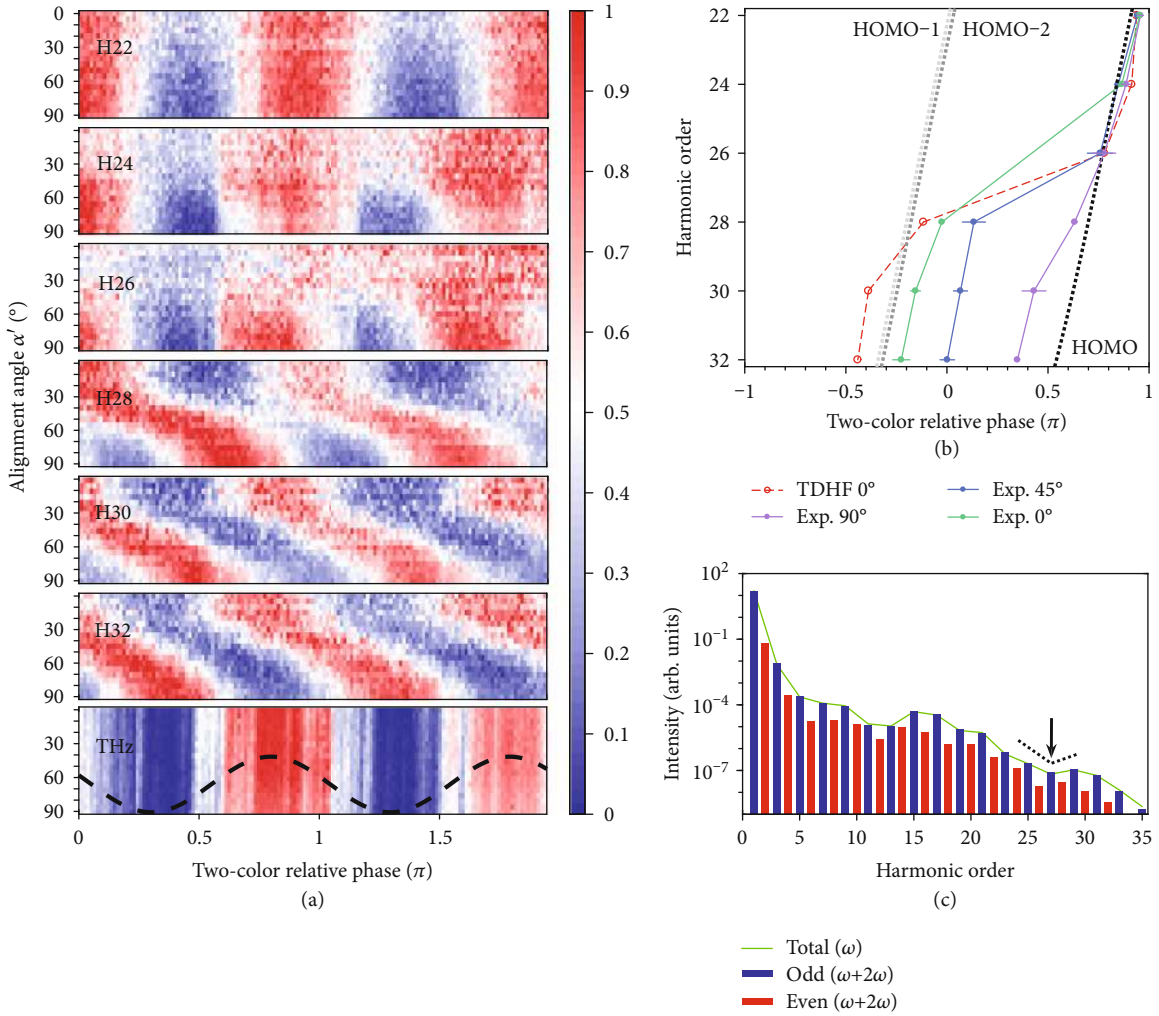

FIGURE 3: Optimal phases of even harmonics determined by molecular attosecond interferometry with THz phase reference. (a) Experimental dependence of high-harmonic and terahertz spectroscopy (HATS) on the alignment angle and two-color relative phase. Intensity modulations of different harmonics are normalized under each alignment angle α', respectively. The black dashed line is the fit of modulation of THz yields. (b) Comparison between the observed optimal phases (OPs) with the parallel (green solid lines), 45-degree (blue solid lines), and perpendicular (violet solid lines) alignments, as well as the calculated OPs considering only the HOMO (black dashed lines), HOMO-1 (light-gray dashed lines), and HOMO-2 (gray dotted lines) channels via the SFA method and the calculated OPs (red open circles) via the time-dependent Hartree-Fock (TDHF) method with parallel alignment. The scales of the error bar are indicated by the horizontal lines. (c) Calculated high-harmonic spectra from parallel-aligned CO_2 when the HOMO, HOMO-1, and HOMO-2 are involved based on the TDHF method. The blue and red bars represent the intensities of odd and even harmonics under two-color fields with the phase delay $\phi = 0$, respectively. The green solid lines show the calculated results under the fundamental field. The black arrow indicates the intensity minimum induced by the interference between HOMO and HOMO-2 channels.

amplitude $E_{\mathrm{THz}}(\alpha')$ is assumed to be proportional to the alignment-dependent ionization probability $N(\alpha')$ [29]. It has been demonstrated that the THz yield takes the maximum at $\phi_{\mathrm{op},T} \approx 0.8\pi$ for atoms and small molecules due to the soft collision of the ionized electron with the ionic core [30]. In the present work, electrons can be released from inner orbitals in spite of their higher ionization potentials [38–40]. The fact that the optimal phase of the THz yields is independent of the alignment angle also indicates no ionization phase difference exists between different ionization channels, in agreement with the previous study [41].

3.2. Molecular Attosecond Interferometry with THz Phase Reference. In Figure 3(a), two-dimensional (2D) measurements of harmonics from H22 to H32 are compared to the robust phase reference of THz yields. The scanning angle step for these 2D measurements is 5 degrees to save the total measurement time. To highlight the two-color phase delay modulation, each horizontal line is normalized by its maxima under each one specific alignment. It can be seen from Figure 3(a) that the OPs for H22 and H24 are almost the same with different alignments, but for the even harmonics higher than H26, a significant phase jump approaching

0.6π can be observed between the parallel and perpendicular alignments, analogous to the results from RABBITT measurement [42]. This can be understood by considering the participation of multiple molecular orbitals [41]. Since no phase variation is observed from the ionization process, the optimal phase for each orbital is determined by the motion of attosecond EWP released from the respective binding orbitals. The optimal phase can be directly mapped to the birth-time of even harmonics [25], reflecting the group delay dispersion of EWPs [43]. Participation of multiple orbitals would modulate the amplitude or phase of the EWP, thus reproducing the angle-dependent OPs. The 2D-measurement opens up avenues for tracing the relative contribution of dominant orbitals by calibrating the intensity modulation of harmonics with the THz phase reference.

The second-harmonic field modifies the phase of the continuum EWP, leading to the modulation of the even harmonics as at each alignment angle $|D_{2N}|^2 \propto \cos^2(\phi - \phi_{\mathrm{op},2N})$ [25, 30], with $\phi_{\mathrm{op},2N}$ being the OPs for the yields of the even harmonics. The explicit values of $\phi_{\mathrm{op},2N}$ can be deduced from fitting the experimental data. In Figure 3(b), the experimentally deduced OPs are presented for H22–H32 with the parallel (0 degree), 45-degree, and perpendicular alignments (90 degrees), respectively. It is worth noting that the absence of OP for H26 in Figure 3(a) around the parallel alignment is because the intensity modulation is too weak to define an explicit value of OP, but the regular modulations clearly reappear around the perpendicular alignment. For comparison, we calculate the OPs assuming the individual involvement of the HOMO, HOMO-1, or HOMO-2. The OP for each orbital is determined by $\phi^s_{\mathrm{op},2N} = -2\omega t_r^{2N}$, where the birth time t_r^{2N} is calculated with strong-field approximation (SFA) [25]. The theoretical predictions of HOMO (ϕ^s_0), HOMO-1 (ϕ^s_1), and HOMO-2 (ϕ^s_2) are shown in Figure 3(b). The OPs of HOMO-1 and HOMO-2 are shifted by π from that of the HOMO due to the phase difference of harmonics emitted from different orbitals (see SM for details). With the robust THz-phase reference, we can confirm that the experimentally deduced OPs for H22 and H24 agree well with the SFA predictions from HOMO. While for harmonics from H28 to H32, a strong deviation occurs between the OPs from the experimental results and the predictions of the HOMO at the parallel alignment. For the other two alignments, we also see the disagreements between experimental results and the prediction with only HOMO involved. At the parallel alignment, the phase jump originates from the optimal phase transition between HOMO and HOMO-2 orbitals with comparable contributions, whereas for the perpendicular alignment, the relatively small phase variation in the OPs between the calculations from HOMO and the experimentally deduced results is attributed to the participation of HOMO-1, which is important in preparing the hole during the ionization step.

To further confirm our analysis, we perform *ab initio* calculations by the time-dependent Hartree-Fock (TDHF) approach [44] for the parallel-aligned CO_2. The OPs at the parallel alignment for harmonics from H22 to H32 experience a significant phase jump across the 26th harmonics, qualitatively agreeing with the measurements in Figure 3(b). The calculated harmonic spectra with the two-color relative phase $\phi = 0$ are shown in Figure 3(c) with the blue and red bars representing the odd- and even-harmonic yields, respectively. By analyzing the individual contribution from each orbital, it is found that the dynamical interference between HOMO and HOMO-2 leads to the spectral minimum and weak modulation around H26 with parallel alignment [41], which is consistent with the experimental results (see SM for details).

3.3. Reconstruction of the Hole Deformation. Based on the molecular attosecond interferometry, the transient hole structure can be reconstructed at the recombination time. The harmonic intensity is proportional to the recombination transition moment between the continuum state $|k\rangle$ and the hole state:

$$D_{2N}(\theta) \propto \left\langle \Psi_{\mathrm{hole}} \middle| \vec{r} \middle| k \right\rangle, \tag{2}$$

with $|\Psi_{\mathrm{hole}}(\theta, t_r^{2N})\rangle = \sum_i |c_i(2N,\theta)| e^{-i\varphi_i(2N,\theta)} |\Psi_i\rangle$ being the hole wave packet at the recombination time. The subscript i labels the orbitals, and we only consider the HOMO ($|\Psi_0\rangle$), HOMO-1 ($|\Psi_1\rangle$), and HOMO-2 ($|\Psi_2\rangle$) of CO_2 in reconstruction of the hole. Recently, numerical investigations suggested a certain contribution of HOMO-3 in the high-harmonic generation from aligned CO_2, and this contribution might become dominant at the cut-off region [45]. In this work, we are dealing with the harmonics in the plateau region; thus, we neglect the contribution of HOMO-3 and only consider the three highest occupied molecular orbitals in reconstructing the hole. To compare with the experimental results directly, the alignment dependence on harmonic yields is considered. The measured even-harmonic yields $M(\alpha', 2N, t_D, \phi)$ could be viewed as the coherent sum among emissions from molecules with different alignments:

$$\begin{aligned} M\left(\alpha', 2N, t_D, \phi\right) &\propto \left| \sum_i A_i\left(\alpha', 2N\right) \cos\left(\phi - \phi_i^s\right) \right|^2 \\ &\simeq \left| \sum_i \left[|c_i(2N,\theta)| e^{-i\varphi_i(2N,\theta)} F_{i,k}\left(\alpha', t_D\right) \right] \cos\left(\phi - \phi_i^s\right) \right|^2, \end{aligned} \tag{3}$$

where $A_i(\alpha', 2N)$ is the fitting amplitude of different molecular orbitals and θ is the polar angle of molecular axis. The experimental results are fitted by the coherent summation of the three involved channels with the dipole matrix element $F_{i,k}(\alpha', t_D)$ integrated with the alignment distribution. The primed and unprimed notations indicate the laboratory frame and molecular frame, respectively. The relative phase difference among the three channels can be determined directly by analyzing the ionization phase, excursion phase, and recombination phase in harmonic generation [41].

The 2D measurements in Figure 3(a) are fitted using Equation (3) with three involved orbitals. It can be seen in

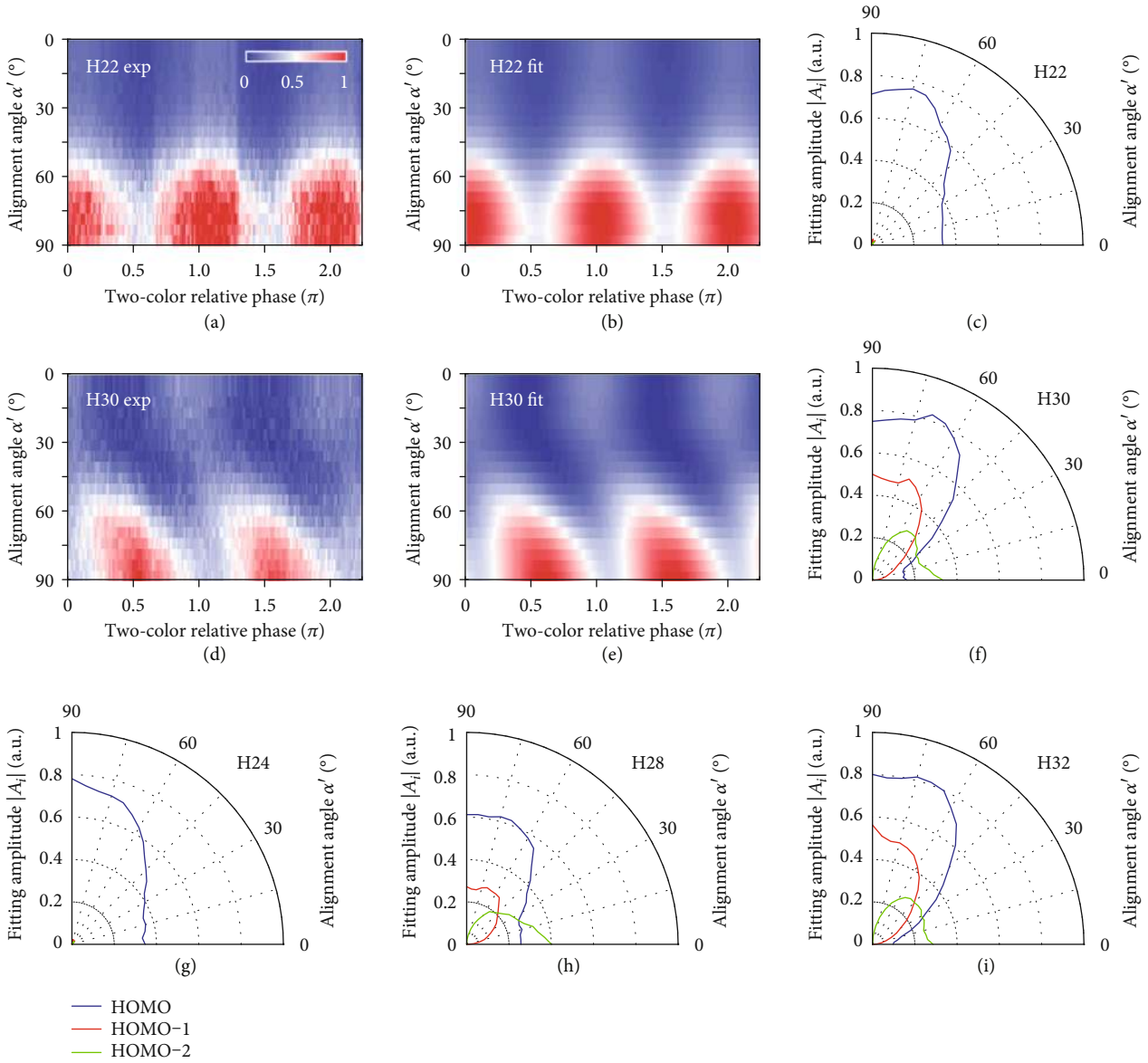

Figure 4: Fitting the participation of different orbitals. Experimental (a) and fitting (b) yields of H22. (c) The fitting amplitudes of HOMO (blue lines), HOMO-1 (red lines), and HOMO-2 (green lines) for H22, shown in polar coordinate. (d–f) present the same for H30. For comparison, we present the fitting amplitudes of the three molecular orbitals for H24 (g), H28 (h), and H32 (i). The standard deviation of the fitting amplitudes $|A_i|$ is estimated to be less than 5%.

Figure 4 that the simulated harmonic yields (Figures 4(b) and 4(e)) are in good agreement with the measurements (Figures 4(a) and 4(d)). The alignment-dependent fitting amplitudes of different orbitals are exhibited in Figures 4(c) and 4(f). The fitting amplitude of the HOMO dominates at all aligned angles for H22 and H24. For H28-H32, the amplitude of HOMO-2 is much greater than the contribution from HOMO for the polar angles less than 30 degrees, resulting in the OP variations from the parallel to the perpendicular alignment.

With the deduced amplitude and phase of each orbital at the recombination time t_r^{2N}, the hole dynamics can be reconstructed by the multi-ionization channels that are inherently coherent. In Figure 5, we show the hole deformation viewed by the EWP with different recolliding momentum k at the parallel and perpendicular alignment angles. Apparently, as the momentum of the recombining electron increases, the hole evolution shows clear transition from the single orbital to the multiple-orbital case at all alignment angles. At the parallel alignment, the reconstructed hole wave packet changes from the HOMO orbital to the HOMO-2-dominated orbital, while at the perpendicular alignment, the hole gradually evolves from the HOMO orbital to a combination of HOMO and HOMO-1 orbitals as a function of the recollision time. The absolute values of the hole wave packet are reconstructed by the coefficients $|c_i|$, the phases φ_i, and the molecular orbitals via applying the expression of hole wave packet in Equation (2), as shown in Figure 5.

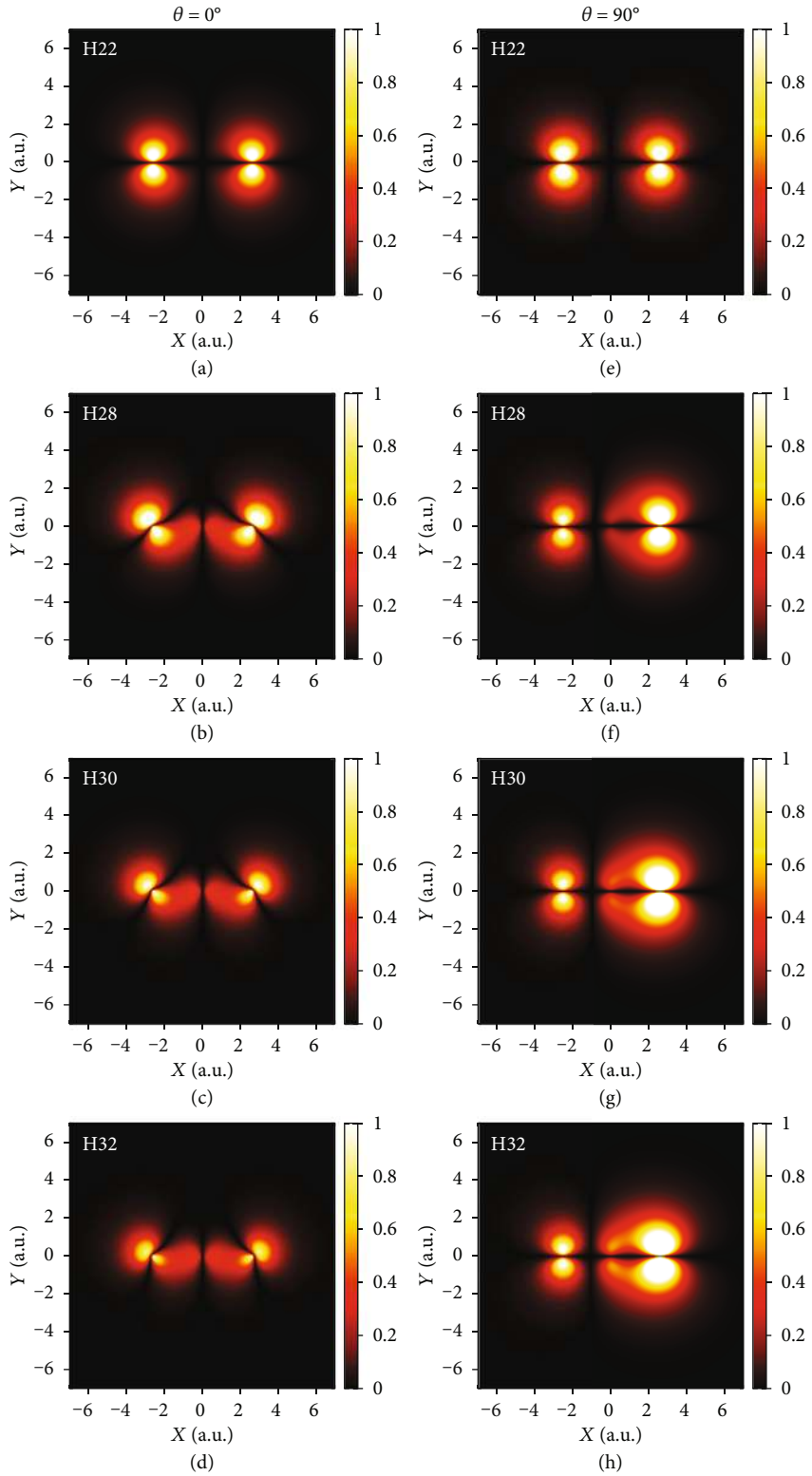

Figure 5: Hole deformation and its dependence on the alignment angle and harmonic order. (a–d) and (e–h) show the normalized holes for parallel and perpendicular alignments, respectively. Columns are sequentially the results of H22, H28, H30, and H32 (from (a) to (d)) for parallel alignment and for perpendicular alignment (from (e) to (h)).

The variation of the hole wave packet reflects the ultrafast dynamics of the coherent molecular ensembles under the strong laser field. Ionization of the ensembles from multi-channels is the first step to create the hole wave packet and the continuum EWP, both of which evolve coherently under the external two-color fields. As the continuum electrons

return to their parent ions at different recombining times, the hole dynamics are recorded by this recombination process with a temporal resolution determined by the time spacing between the neighboring two harmonics. For an electron with a smaller momentum, it mainly sees the contribution of the HOMO orbital to the hole wave packet, whereas for an electron with a larger momentum, the inner orbitals can contribute to the formation of the hole. Therefore, the control of a hole wave packet via different alignments of molecular ensembles can be revealed here by the hole dynamics in Figure 5. Strong-field ionization creates the angle-dependent hole wave packet, and the hole dynamics at different alignment angles are determined by the amplitude and the phase of the participated orbital. The hole shape reconstructed from harmonic H22 keeps almost the same for all alignment angles, because the optimal phase for H22 keeps constant in the experimental results; therefore, the reconstructed hole wave packet is mainly contributed by the HOMO orbital. The slight differences in the absolute values of the hole wave packet between different alignments reflect the angular-dependent ionization probabilities. The hole recorded by the higher harmonics exhibits a strong alignment-dependent deformation, which can be directly observed from the reconstructed hole in Figure 5. The shape of the hole gradually changes from a σ-dominant orbital to a π-dominant orbital from the parallel to the perpendicular alignment, reflecting the geometry of the participating orbitals. Meanwhile, the angle-dependent phase variation observed at higher harmonics indicates that the recombination time depends on the alignment angle for electrons with the same recolliding momentum, which is about 400 attoseconds earlier at the perpendicular alignment than the parallel alignment, reflecting the angle dependence of correlation between the EWP and the ionic core. The hole shapes reconstructed by the phase of even harmonics from H28 to H32 exhibit a strong alignment dependence, implying a possible control on the hole by selecting the involved orbitals via different ionization angles.

4. Discussion

The present research demonstrates how to probe the ultrafast deformation of a molecular hole from threefold control using molecular attosecond interferometry. The impulsive alignment of the molecule is achieved by creating a coherent molecular rotational wave packet by rotational Raman transitions and fixing the molecule axis in the laboratory frame. The opposite two arms of the propagating directions are used to form the interferometry of electrons, and the relative phase can be adjusted by a weak second-harmonic pulse in a resolution of several tens of attoseconds. By jointly measuring the second-harmonic pulse-modulated HATS, harmonic phases and the hole dynamics are precisely extracted with the robust phase reference of the modulated THz yields. Harmonics with alignment-dependent OPs imply alignment-dependent participation of different orbitals. By fitting the amplitudes of these orbitals, it is possible to reconstruct the hole dynamics, as demonstrated in Figure 5. Moreover, we note that the evolution of EWP can also be decoded in the phase variation observed from the molecular attosecond interferometry.

These results suggest a precise control over hole dynamics at the attosecond timescale and subangstrom space-scale resolutions. The state-of-the-art ultrafast processes, such as the hole carrier, thermal, and acoustic dynamics in condensed matter, have been investigated by nanoscale pump-probe detection [46, 47]. However, we are dealing with a faster process, which occurs within a fraction of one laser cycle from the phase-matched molecules. Although hole dynamics is previously studied from the yields of different orders of harmonics [11], our methodology can provide more precise control over the initial formation and retrieve detailed information on the following dynamics of the hole-electron system, thanks to the HATS technique.

A hole is a left vacant of an absent electron. Previously, the structural deformation of CO_2 molecules was reported in the presence of strong laser fields, and it was interpreted by the coupling between the electronically excited and ground states of ions [48]. Because different molecular states are close to each other in energy spacing, under the exposure of laser pulses, multimolecular states can be excited. These electrons, ejected from not only the HOMO but also the inner orbitals, are released creating a coherent EWP, which is the coherent superposition of electronic eigenstates. The remaining hole, which is a mixture of different one-hole configurations, can exhibit a time-dependent deformation that reflects the coherent nature between different states [11]. Hole deformation can also be controlled by varying the alignment angle of an ensemble of molecules due to the alignment-dependent ionization of different orbitals [21]. In the present work, we experimentally and theoretically advance this concept. The dispersion of the recombined EWP can be precisely tuned by the phase difference between the two-color laser fields, which helps to add a new dimension of detection. Different from the previous research of hole which detects only the intensities and phases of different harmonics and therefore confirms the participation of HOMO and HOMO-1 of N_2 [49], our molecular attosecond interferometry can add an additional phase of the EWP, leading to the reconstruction of hole deformation from more than two orbitals. In other words, our method can be applied to the other polyatomic molecules that exhibit the alignment-dependent ionization channels, for instance, N_2O_4 [50], C_4H_6, C_4H_{10} [51], C_2HI [11], C_2H_2 [52, 53], CF_3I [54], and COS [55], in order to understand the channel-dependent dynamics during the strong field process. So far, the present work is limited to study the electron dynamics decoupled with nuclear motion. More fields of study, such as the vibrational dynamics [50, 56] and the coupling between electrons and nuclear [7, 8, 53, 57], can benefit from our method when using pulses with shorter pulse duration. Furthermore, we expect that the molecular attosecond interferometry based on the precise control of rotational and electronic wave packets and laser shaping will advance the study of ultrafast electron correlations and multidimensional and multichannel couplings in a range of fields,

such as chemical reactions, molecular orbital tomography, charge migration, and transport.

Data Availability

The data that support the findings of this study are available from the corresponding author upon reasonable request.

Conflicts of Interest

The authors declare that there is no conflict of interest regarding the publication of this article.

Authors' Contributions

J.Y. and Z.Z. conceived the idea. Y.H., X.W., Z.L., D.Z., and Z.Z. designed and conducted the experiments. Y.H., J.Z., Z.S., J.C., J.Y., and Z.Z. analyzed the data. J.Z., Z.S., Y.Z., J.L., and W.D. carried out the calculations. All authors discussed the results and contributed to the writing of the manuscript. Yindong Huang, Jing Zhao, and Zheng Shu contributed equally to this work.

Acknowledgments

J.Z. and Z.Z. acknowledge Prof. Manfred Lein for the helpful discussions. This work was supported by the National Key Research and Development Program of China (Grant Nos. 2019YFA0307703, 2019YFA0307700, and 2016YFA0401100), the Major Research Plan of the National Natural Science Foundation of China (Grant No. 91850201), and the National Natural Science Foundation of China (Grant Nos. 11804388, 11874066, 11904400, U1830206, and 11974426).

Supplementary Materials

Experimental setup, channel-resolved quantum-orbit analysis for optimal phases of HHG, data analysis by fitting the intensity modulations, and time-dependent Hartree-Fock approach. Figure S1: the detailed experimental setup. Figure S2: quantum-orbit analysis for the optimal phases of different harmonics under the Strong Field Approximation (SFA). Figure S3: the recombination dipole moments of HOMO, HOMO-1, and HOMO-2 orbitals of CO_2 and the corresponding orbitals. Figure S4: The normalized harmonic-order-dependent coefficients $|c_i(2N, \theta)|$. Figure S5: harmonic spectra calculated by the time-dependent Hartree-Fock approach (TDHF) method. Figure S6: experimentally observed high harmonic spectra with the phase delay $\phi = 0$ under the parallel, 45-degree, and perpendicular alignment. *(Supplementary Materials)*

References

[1] M. Dantus, M. J. Rosker, and A. H. Zewail, "Real-time femtosecond probing of "transition states" in chemical reactions," *The Journal of Chemical Physics*, vol. 87, no. 4, pp. 2395–2397, 1987.

[2] M. J. Rosker, M. Dantus, and A. H. Zewail, "Femtosecond clocking of the chemical bond," *Science*, vol. 241, no. 4870, pp. 1200–1202, 1988.

[3] A. Mokhtari, P. Cong, J. L. Herek, and A. H. Zewail, "Direct femtosecond mapping of trajectories in a chemical reaction," *Nature*, vol. 348, no. 6298, pp. 225–227, 1990.

[4] A. H. Zewail, "Femtochemistry: atomic-scale dynamics of the chemical bond," *The Journal of Physical Chemistry*, vol. 104, no. 24, pp. 5660–5694, 2000.

[5] A. D. Bandrauk, S. Chelkowski, P. B. Corkum, J. Manz, and G. L. Yudin, "Attosecond photoionization of a coherent superposition of bound and dissociative molecular states: effect of nuclear motion," *Journal of Physics B: Atomic Molecular & Optical Physics*, vol. 42, no. 13, article 134001, 2009.

[6] M. Kowalewski, K. Bennett, J. R. Rouxel, and S. Mukamel, "Monitoring nonadiabatic Electron-Nuclear dynamics in molecules by attosecond streaking of photoelectrons," *Physical Review Letters*, vol. 117, no. 4, pp. 43–201, 2016.

[7] C. Arnold, O. Vendrell, and R. Santra, "Electronic decoherence following photoionization: full quantum-dynamical treatment of the influence of nuclear motion," *Physical Review A*, vol. 95, no. 3, article 033425, 2017.

[8] D. Jia, J. Manz, and Y. Yang, "De- and recoherence of charge migration in ionized iodoacetylene," *The Journal of Physical Chemistry Letters*, vol. 10, no. 15, pp. 4273–4277, 2019.

[9] P. M. Paul, E. S. Toma, P. Breger et al., "Observation of a train of attosecond pulses from high harmonic generation," *Science*, vol. 292, no. 5522, pp. 1689–1692, 2001.

[10] F. Calegari, D. Ayuso, A. Trabattoni et al., "Ultrafast electron dynamics in phenylalanine initiated by attosecond pulses," *Science*, vol. 346, no. 6207, pp. 336–339, 2014.

[11] P. M. Kraus, B. Mignolet, D. Baykusheva et al., "Measurement and laser control of attosecond charge migration in ionized iodoacetylene," *Science*, vol. 350, no. 6262, pp. 790–795, 2015.

[12] L. Cattaneo, J. Vos, R. Y. Bello et al., "Attosecond coupled electron and nuclear dynamics in dissociative ionization of H2," *Nature Physics*, vol. 14, no. 7, p. 733, 2018.

[13] N. V. Golubev, T. Begusic, and J. Vanicek, "On-the-fly ab initio semiclassical evaluation of electronic coherences in polyatomic molecules reveals a simple mechanism of decoherence," *Physical Review Letters*, vol. 125, no. 8, article 083001, 2020.

[14] L. L. Patera, F. Queck, P. Scheuerer, and J. Repp, "Mapping orbital changes upon electron transfer with tunnelling microscopy on insulators," *Nature*, vol. 566, no. 7743, pp. 245–248, 2019.

[15] M. Nisoli, P. Decleva, F. Calegari, A. Palacios, and F. Martin, "Attosecond electron dynamics in molecules," *Chemical Reviews*, vol. 117, no. 16, pp. 10760–10825, 2017.

[16] S. Haessler, J. Caillat, and P. Salieres, "Self-probing of molecules with high harmonic generation," *Journal of Physics B: Atomic, Molecular and Optical Physics*, vol. 44, no. 20, article 203001, 2011.

[17] A. J. Uzan, H. Soifer, O. Pedatzur et al., "Spatial molecular interferometry via multidimensional high-harmonic spectroscopy," *Nature Photonics*, vol. 14, no. 3, pp. 188–194, 2020.

[18] P. B. Corkum, "Plasma perspective on strong field multiphoton ionization," *Physical Review Letters*, vol. 71, no. 13, pp. 1994–1997, 1993.

[19] T. Okino, Y. Furukawa, Y. Nabekawa et al., "Direct observation of an attosecond electron wave packet in a nitrogen molecule," *Science Advances*, vol. 1, no. 8, article e1500356, 2015.

[20] H. Eyring, J. Walter, and G. E. Kimball, *Quantum Chemistry*, New York, NY, USA, Wiley, 1944.

[21] O. Smirnova, S. Patchkovskii, Y. Mairesse, N. Dudovich, and M. Y. Ivanov, "Strong-field control and spectroscopy of attosecond electron-hole dynamics in molecules," *Proceedings of the National Academy of Sciences of the United States of America*, vol. 106, no. 39, pp. 16556–16561, 2009.

[22] T. Lu and F. Chen, "Multiwfn: a multifunctional wavefunction analyzer," *Journal of Computational Chemistry*, vol. 33, no. 5, pp. 580–592, 2012.

[23] A. T. Le, X. M. Tong, and C. D. Lin, "Alignment dependence of high-order harmonic generation from CO_2," *Journal of Modern Optics*, vol. 54, no. 7, pp. 967–980, 2007.

[24] L. He, P. Lan, A.-T. Le et al., "Real-time observation of molecular spinning with angular high-harmonic spectroscopy," *Physical Review Letters*, vol. 121, no. 16, article 163201, 2018.

[25] N. Dudovich, O. Smirnova, J. Levesque et al., "Measuring and controlling the birth of attosecond XUV pulses," *Nature Physics*, vol. 2, no. 11, pp. 781–786, 2006.

[26] O. Pedatzur, G. Orenstein, V. Serbinenko et al., "Attosecond tunnelling interferometry," *Nature Physics*, vol. 11, no. 10, pp. 815–819, 2015.

[27] B. K. McFarland, J. P. Farrell, P. H. Bucksbaum, and M. Guhr, "High harmonic generation from multiple orbitals in N_2," *Science*, vol. 322, no. 5905, pp. 1232–1235, 2008.

[28] F. Schell, T. Bredtmann, C. P. Schulz, S. Patchkovskii, M. J. J. Vrakking, and J. Mikosch, "Molecular orbital imprint in laser-driven electron recollision," *Science Advances*, vol. 4, no. 5, article eaap8148, 2018.

[29] Y. Huang, C. Meng, X. Wang et al., "Joint measurements of terahertz wave generation and high-harmonic generation from aligned nitrogen molecules reveal angle-resolved molecular structures," *Physical Review Letters*, vol. 115, no. 12, article 123002, 2015.

[30] D. Zhang, Z. Lu, C. Meng et al., "Synchronizing terahertz wave generation with attosecond bursts," *Physical Review Letters*, vol. 109, no. 24, article 243002, 2012.

[31] P. M. Kraus, M. Zurch, S. Cushing, D. M. Neumark, and S. R. Leone, "The ultrafast x-ray spectroscopic revolution in chemical dynamics," *Nature Reviews Chemistry*, vol. 2, no. 6, pp. 82–94, 2018.

[32] C. Vozzi, M. Negro, F. Calegari et al., "Generalized molecular orbital tomography," *Nature Physics*, vol. 7, no. 10, pp. 822–826, 2011.

[33] D. Pavicic, K. F. Lee, D. M. Rayner, P. B. Corkum, and D. M. Villeneuve, "Direct measurement of the angular dependence of ionization for N_2, O_2, and CO_2 in intense laser fields," *Physical Review Letters*, vol. 98, no. 24, article 243001, 2007.

[34] I. Thomann, R. Lock, V. Sharma et al., "Direct measurement of the angular dependence of the single-photon ionization of aligned N_2 and CO_2," *The Journal of Physical Chemistry A*, vol. 112, no. 39, pp. 9382–9386, 2008.

[35] S.-K. Son and S.-I. Chu, "Multielectron effects on the orientation dependence and photoelectron angular distribution of multiphoton ionization of CO2 in strong laser fields," *Physical Review A*, vol. 80, no. 1, article 011403, 2009.

[36] M. Abu-samha and L. B. Madsen, "Theory of strong-field ionization of aligned CO_2," *Physical Review A*, vol. 80, no. 2, article 023401, 2009.

[37] S.-F. Zhao, C. Jin, A. T. Le, T. F. Jiang, and C. D. Lin, "Analysis of angular dependence of strong-field tunneling ionization for CO2," *Physical Review A*, vol. 80, no. 5, article 051402, 2009.

[38] V. P. Majety and A. Scrinzi, "Dynamic exchange in the strong field ionization of molecules," *Physical Review Letters*, vol. 115, no. 10, article 103002, 2015.

[39] C. Jin, A.-T. Le, and C. D. Lin, "Analysis of effects of macroscopic propagation and multiple molecular orbitals on the minimum in high-order harmonic generation of aligned CO_2," *Physical Review A*, vol. 83, no. 5, article 053409, 2011.

[40] P. Krause and H. B. Schlegel, "Angle-dependent ionization of small molecules by time-dependent configuration interaction and an absorbing potential," *The Journal of Physical Chemistry Letters*, vol. 6, no. 11, pp. 2140–2146, 2015.

[41] O. Smirnova, Y. Mairesse, S. Patchkovskii et al., "High harmonic interferometry of multi-electron dynamics in molecules," *Nature*, vol. 460, no. 7258, pp. 972–977, 2009.

[42] W. Boutu, S. Haessler, H. Merdji et al., "Coherent control of attosecond emission from aligned molecules," *Nature Physics*, vol. 4, no. 7, pp. 545–549, 2008.

[43] Y. Mairesse, A. de Bohan, L. J. Frasinski et al., "Attosecond synchronization of high-harmonic soft x-rays," *Science*, vol. 302, no. 5650, pp. 1540–1543, 2003.

[44] S. Hu, Z. Zhao, J. Chen, and T. Shi, "Ionization dynamics of C_2H_2 in intense laser fields: time-dependent Hartree-Fock approach," *Physical Review A*, vol. 92, no. 5, article 053409, 2015.

[45] M. Ruberti, P. Decleva, and V. Averbukh, "Multi-channel dynamics in high harmonic generation of aligned CO_2: ab initio analysis with time-dependent b-spline algebraic diagrammatic construction," *Physical Chemistry Chemical Physics*, vol. 20, no. 12, pp. 8311–8325, 2018.

[46] Y. Terada, S. Yoshida, O. Takeuchi, and H. Shigekawa, "Real-space imaging of transient carrier dynamics by nanoscale pump-probe microscopy," *Nature Photonics*, vol. 4, no. 12, pp. 869–874, 2010.

[47] R. M. Karl Jr., G. F. Mancini, J. L. Knobloch et al., "Full-field imaging of thermal and acoustic dynamics in an individual nanostructure using tabletop high harmonic beams," *Science Advances*, vol. 4, no. 10, article eaau4295, 2018.

[48] S. Minemoto, T. Kanai, and H. Sakai, "Alignment dependence of the structural deformation of CO_2 molecules in an intense femtosecond laser field," *Physical Review A*, vol. 77, no. 4, article 041401, 2008.

[49] S. Haessler, J. Caillat, W. Boutu et al., "Attosecond imaging of molecular electronic wavepackets," *Nature Physics*, vol. 6, no. 3, pp. 200–206, 2010.

[50] W. Li, X. Zhou, R. Lock et al., "Time-resolved dynamics in N_2O_4 probed using high harmonic generation," *Science*, vol. 322, no. 5905, pp. 1207–1211, 2008.

[51] A. E. Boguslavskiy, J. Mikosch, A. Gijsbertsen et al., "The multielectron ionization dynamics underlying attosecond strong-field spectroscopies," *Science*, vol. 335, no. 6074, pp. 1336–1340, 2012.

[52] M. G. Pullen, B. Wolter, A.-T. Le et al., "Imaging an aligned polyatomic molecule with laser-induced electron diffraction," *Nature Communications*, vol. 6, no. 1, article 7262, 2015.

[53] B. Wolter, M. G. Pullen, A.-T. Le et al., "Ultrafast electron diffraction imaging of bond breaking in di-ionized acetylene," *Science*, vol. 354, no. 6310, pp. 308–312, 2016.

[54] F. Krečinić, P. Wopperer, B. Frusteri et al., "Multiple-orbital effects in laser-induced electron diffraction of aligned molecules," *Physical Review A*, vol. 98, no. 4, article 041401, 2018.

[55] A. Trabattoni, J. Wiese, U. D. Giovannini et al., "Setting the photoelectron clock through molecular alignment," *Nature Communications*, vol. 11, no. 1, article 2546, 2020.

[56] P. M. Kraus, S. B. Zhang, A. Gijsbertsen, R. R. Lucchese, N. Rohringer, and H. J. Worner, "High-harmonic probing of electronic coherence in dynamically aligned molecules," *Physical Review Letters*, vol. 111, article 243005, p. 24, 2013.

[57] Y. Kobayashi, K. F. Chang, S. M. Poullain et al., "Coherent electronic-vibrational dynamics in deuterium bromide probed via attosecond transient-absorption spectroscopy," *Physical Review A*, vol. 101, no. 6, article 63414, 2020.